Study of thermal pressure and phase transitions in H_2O using optical pressure sensors in the diamond anvil cell

2004 J. Phys.: Condens. Matter 16 S1223

(http://iopscience.iop.org/0953-8984/16/14/034)

INSTITUTE OF PHYSICS PUBLISHING JOURNAL OF PHYSICS: CONDENSED MATTER

J. Phys.: Condens. Matter **16** (2004) S1223–S1233 PII: S0953-8984(04)74963-2

Study of thermal pressure and phase transitions in H_2O using optical pressure sensors in the diamond anvil cell

Sara Sundberg and Peter Lazor

Department of Earth Sciences, Uppsala University, S-752 36 Uppsala, Sweden

E-mail: Sara.Sundberg@geo.uu.se and Peter.Lazor@geo.uu.se

Received 22 January 2004
Published 26 March 2004
Online at stacks.iop.org/JPhysCM/16/S1223
DOI: 10.1088/0953-8984/16/14/034

Abstract

We present results of a study on the phase equilibria and pressure–volume–temperature relations for water and ice VII using an optical system designed for Raman spectroscopy and pressure–temperature measurements. The study shows that the strontium borate sensor represents an important tool for high-pressure–high-temperature manometry for temperatures below 600 K. In the pressure–temperature ranges 0–5 GPa and 240–600 K we detected phase transformations between four phases of H_2O as documented by Raman spectra, pressure–temperature scans, and visual observations. Analysis of the interference fringes and comparison of the experimental data on thermal pressure with the published equations of state (EOSs) show that the heating/cooling cycles were carried out under quasi-isochoric conditions. The experimental results are discussed/analysed on the basis of different EOSs for water and ice.

1. Introduction

Studies of H_2O ice phases and the behaviour of liquid water under high-pressure, high-temperature conditions are important for several different reasons. Liquid water is of great geological interest because water-rich fluids are abundant in the interior of the Earth [1]. The study of the high-pressure phases of H_2O ice is important, too. Although ice is not stable in the hot interior of the Earth, high-pressure ices may exist temporarily in cold subducting slabs [2]. In the outer Solar System, ices represent major constituents of mantles of Jovian planets and control mineralogies of icy satellites [3, 4]. These satellites are covered by thick ice sheets and there is indirect evidence that they may possess subsurface liquid oceans [5, 6]. Properties of ices and water at extreme conditions are also of great importance for solid state physics and chemistry, where they represent an important class of hydrogen-bonded materials.

Table 1. List of equations of state for water and ice VII used in this study.

Equation of state	Temperature range (K)	Pressure range (GPa)
Water		
[10]	374–2000	0–10
[12]	Up to 3000	>0.2
[11]	273.16–623	0–20
[14]	373–1273	0.002–5
[9]	373–1873	0.0001–5
[8]	273–473	0–3.5
[7]	Melting line to 1273	0–25
Ice VII		
[20]	300–700	6–20

In this study we report results on the high-pressure investigation of H_2O using an optical system designed for Raman and pressure–temperature measurements. We collected experimental pressure and temperature data, and high-quality Raman spectra in the 0–5 GPa and 240–600 K ranges. The high resolution of our measurements carried out in the quasi-isochoric conditions allowed detection of phase transitions and evaluation of thermal pressures during heating/cooling cycles. Four phases of H_2O have been observed: water, and ices VI, VII, and VIII. Ice VI has a tetragonal structure and is the stable phase of H_2O from 0.9 to 2.2 GPa at room temperature, whereas ice VII has a proton-disordered cubic structure and is stable in excess of 2.2 GPa. Upon cooling below 278 K, ice VII transforms to a proton-ordered ice VIII.

Through this study, we compare several published equations of state (EOSs) listed in table 1 to the experimental pressure–temperature data. The Saul and Wagner [7] EOS is a fundamental equation based on the Helmholtz function fitted to various experimental data. This equation covers the entire fluid region from the melting line to 1273 K and 25 GPa. The Wiryana *et al* [8] equation is based on sound velocities in liquid water and their function of temperature and pressure. This equation is determined at up to 473 K and 3.5 GPa. The Holland and Powell [9] EOS is an extension of the modified Redlich–Kwong (MRK) equation. Virial-type terms are added to enlarge the field of its applicability to cover the range 0–5 GPa and 373–1873 K. The Pitzer and Sterner [10] EOS is fitted to data over the entire range from vapour and liquid below the critical temperature to at least 2000 K and from zero to more than 10 GPa. The Rimbach and Chatterjee [11] equation is an MRK-type equation valid in the ranges 273–623 K and 0–20 GPa. The Saxena and Fei equation [12, 13] is a virial-type equation of state valid up to 3000 K and above 0.2 GPa. The Halbach and Chatterjee [14] equation is an empirically derived Redlich–Kwong type of EOS valid in the range 373–1273 K and 0.002–5 GPa.

2. Experimental details

2.1. Sample preparation

A diamond anvil cell (DAC) of a piston–cylinder design (Mao–Bell type) was used in the experiments. The cell was loaded with a sample of distilled, deionized water (resistivity 18 MΩ cm) and two optical pressure sensors: ruby—$Al_2O_3:Cr^{3+}$—and strontium borate—

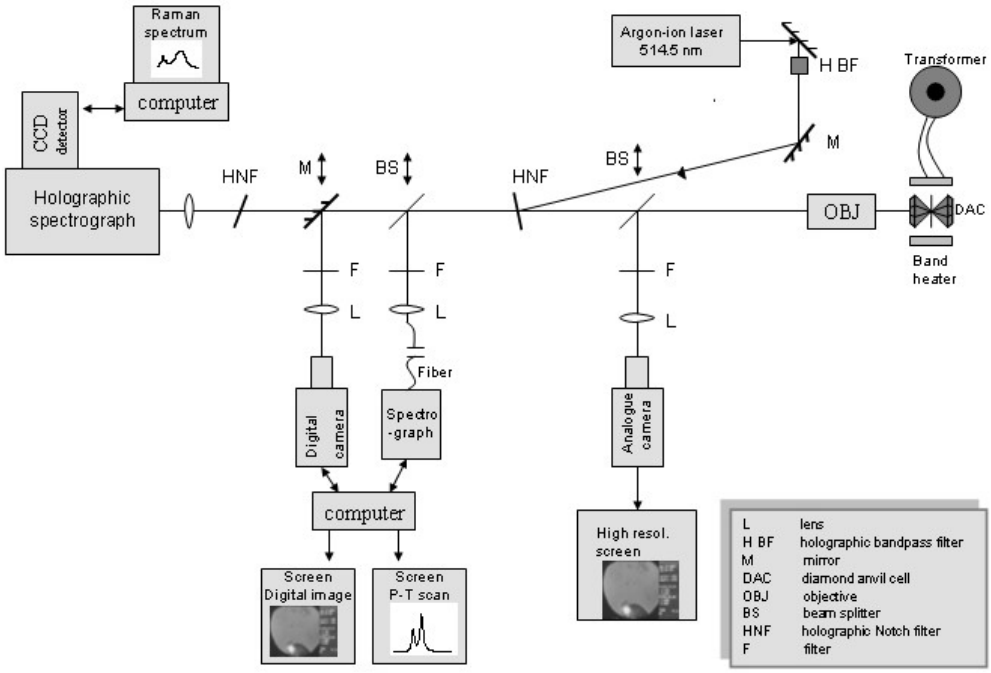

Figure 1. Set-up for Raman and pressure–temperature measurement.

SrB_4O_7:Sm^{2+}. Rhenium foil of 250 μm thickness, preindented to 70 μm, served as a gasket material. The diameter of the sample chamber was 200 μm at the beginning of the experiments.

2.2. Experimental set-up

We used combined Raman and pressure–temperature measurement systems specially designed for studying phase equilibria in H_2O by the DAC technique (figure 1). The Raman system consists of an imaging spectrometer (HoloSpec, Kaiser) equipped with a holographic transmission grating (HoloPlex) and thermoelectrically cooled CCD detector (Andor). The grating simultaneously disperses two separate spectral tracks onto the CCD detector, which results in a Raman spectrum over a very broad spectral range from -250 to 5000 cm^{-1} with spectral resolution of 4 cm^{-1}, obtained in one single acquisition. This is of a great advantage when carrying out high-pressure–high-temperature experiments on H_2O. A wide wavenumber range, which includes both high-wavenumber intramolecular vibrations and low-wavenumber translational–librational modes, is collected under the same pressure–temperature conditions (figure 2). Raman emission was excited in the back-scattering geometry by the 514.5 nm line of an argon-ion laser providing up to 50 mW of power. The Rayleigh line and stray light were efficiently rejected by two holographic notch filters (Kaiser). Typical integration time varied between 5 and 15 min.

Temperature changes during the heating/cooling cycles were controlled with a band heater (Tempco) wrapped around the DAC and connected to a variable transformer (figure 1). Subfreezing temperatures (down to 230 K) were achieved by cooling the DAC with a cold finger attached to the chiller (CryoCool, Neslab). To measure the temperature a K-type thermocouple (uncertainty ± 1 K) was attached to each diamond.

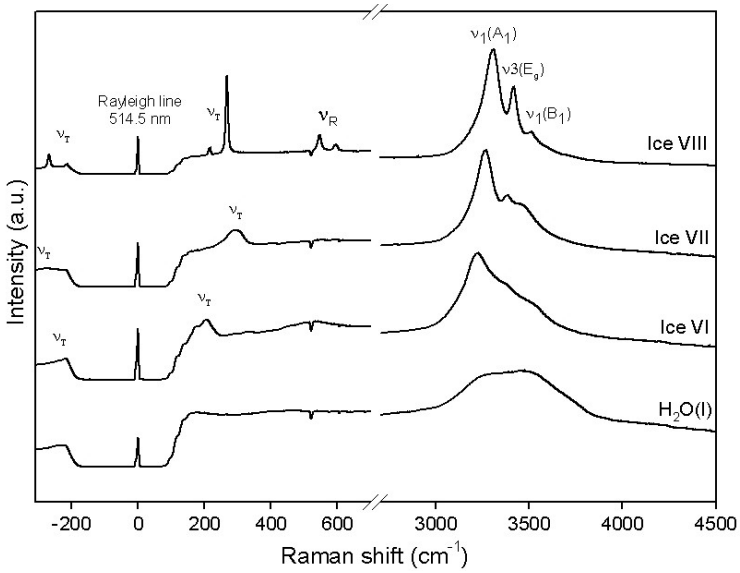

Figure 2. Raman spectra of H_2O phases. H_2O (l), 0.6 GPa, 298 K; ice VI, 1.3 GPa, 298 K; ice VII, 298 K, 4.2 GPa; ice VIII, ∼3.5 GPa, 254 K.

The fluorescence spectra from the two optical pressure sensors (figure 3) as well as the high-resolution digital images were continuously recorded during the temperature variation. The information from the optical sensors (peak positions of lines ruby R1 and strontium borate $^7D_0 - {}^5F_0$) along with the temperature readings were processed in a manner described by Datchi *et al* [15] and yielded accurate pressure–temperature paths followed by the sample of H_2O during the heating/cooling cycles. A typical pressure uncertainty—precision—arising from the standard deviation of one peak-fitting procedure was about 0.01–0.02 GPa both for the ruby and borate sensors (reported in figure 3). This value translated to a thermal pressure precision of about 0.002 GPa (at 95% confidence level) when a series of p–T points (>20 points) forming the p–T paths was fitted by a simple linear/quadratic function. Although the true uncertainty—accuracy—is much higher (on the order of few tenths of a gigapascal) it is the precision that matters for the determination of thermal pressure, which is evaluated as the difference between two pressure values. The p–T paths and the recorded optical observations were always kept synchronized so that, at any moment, visual changes could be related to the p–T path features (discontinuities, slope changes) and vice versa.

The $SrB_4O_7:Sm^{2+}$ pressure sensor was proposed in pioneering work by Lacam and Chateau [16]. The great advantage of this sensor is that the temperature-induced shift of its luminescence (-0.01 Å K^{-1}) is about 70 times smaller than the shift of the ruby sensor [15]. On the other hand, we observed that at higher temperatures (>600 K) the $SrB_4O_7:Sm^{2+}$ sensor becomes somewhat more susceptible to the reaction with H_2O and deteriorates [17].

As a result of the mutual proximity of the ruby and strontium borate crystals in the sample chamber (figure 4(d)) it was possible to collect simultaneously fluorescence spectra from both sensors (figure 3). The redundant information from the two sensors and the weak temperature dependence of the luminescence of strontium borate allowed determination of temperatures even without the thermocouple readings using the formula derived by Datchi *et al* [15]. Two pressure readings, the strontium borate based and the ruby based, were obtained, too. Figure 3 contains an example of two p–T sets determined from the peak positions in the spectrum

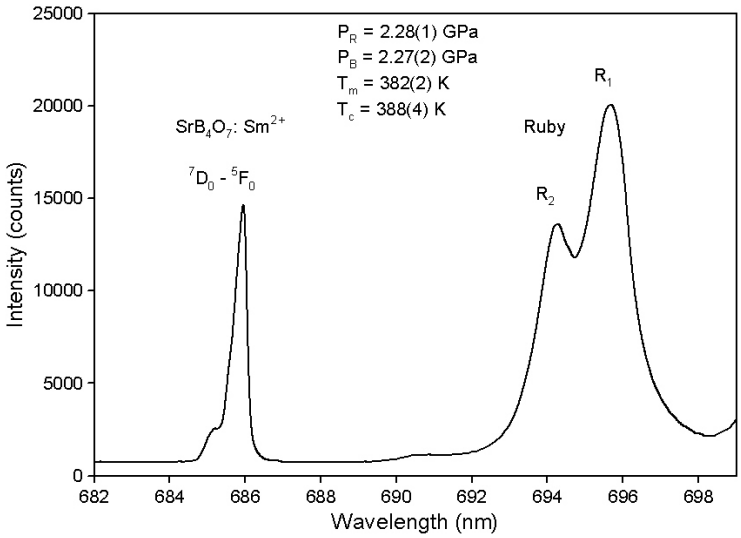

Figure 3. Fluorescence lines from the optical sensors, strontium borate and ruby. T_m is the temperature measured from thermocouples; T_c is the temperature calculated combining the fluorescence lines of both sensors using the metrology of Datchi *et al* [15]. P_R is pressure measured from ruby and P_B pressure measured from strontium borate.

and from the thermocouple readings. The small differences originates from a combination of several factors, which may include the calibration of sensors, different state of sensor stress, fitting errors, and effects of temperature gradient, as well as from the accuracy of thermocouple readings. The pressures and temperatures reported in this study and used for the calculations are based on the shifts of the fluorescence line of the strontium borate sensor and on the thermocouple readings, respectively.

2.3. Experimental procedures

Two types of experiment have been conducted: heating/cooling experiments and Raman spectroscopy.

In a typical heating/cooling experiment, the pressure was fixed at a chosen nominal value (between 0.5 and 5 GPa) and temperature was increased/decreased in the range 300–500 K. Figure 5 shows several typical p–T paths recorded during heating/cooling cycles. We attribute the major part of the change of pressure due to the effect of thermal pressure, which occurs upon a temperature change at the quasi-isochoric conditions in the sample chamber. The conditions for the isochoricity were tested using the method of interference fringes. Figure 6 shows two interference patterns recorded from the compressed liquid water at 323 and 373 K. We calculated the thickness of the sample chamber from the wavelength separation of maxima and minima of fringes and using the volume dependence of refractive index of water determined by Dewaele *et al* [18]. The temperature and wavelength dependences of refractive index have not been considered. Their effects on the results are at least one order of magnitude smaller than the density effect (in order to minimize the effect of dispersion we used only up to four neighbouring fringes for the thickness calculation). The results indicate a slight decrease of thickness of the confined layer of liquid water by about 0.15(20) μm (from 61.46 to 61.31 μm; $\sim$0.24%) upon cooling down by 50 K. According to the p–V–T EOS of liquid water provided by Saul and Wagner [7], an isothermal change of volume of this magnitude corresponds to a

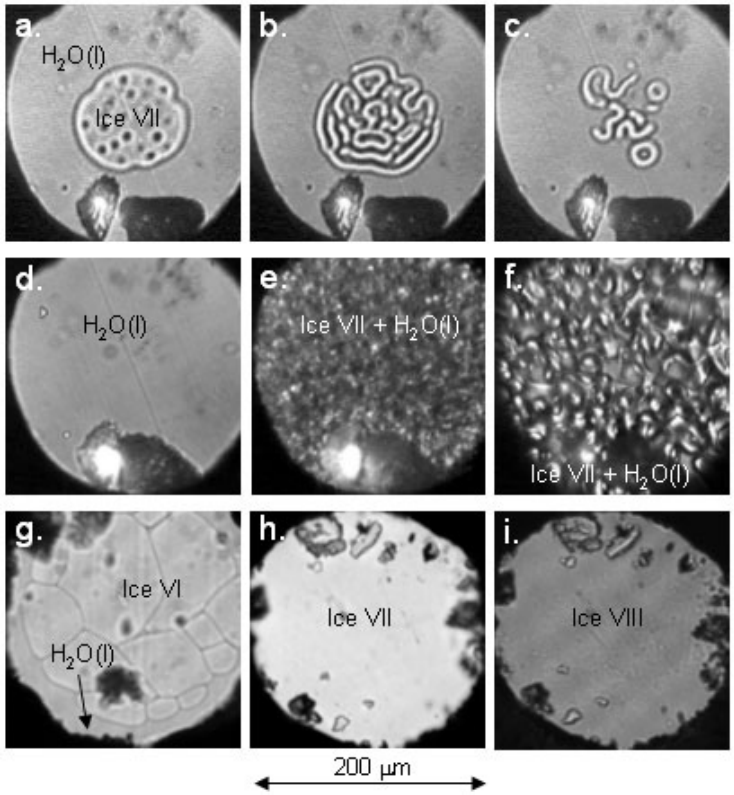

Figure 4. (a)–(c) Melting of ice VII, $P = 3.3$ GPa, $T = 447$ K (experiment w7 in figure 5); (d)–(f) freezing of ice VII, $T = 390$ K; on freezing pressure drops from 3.5 to 2.6 GPa (experiment w8 in figure 5); (g) equilibrium between ice VI and H_2O (l), $P \sim 2$ GPa, $T = 350$ K; (h) ice VII, $P = 3.48$ GPa, $T = 298$ K; (i) ice VIII, $P \sim 3.5$ GPa, $T = 254$ K.

pressure change (increase) of about 0.03 GPa. Within the method's accuracy, the examination of the high-quality digital images did not reveal any change in the lateral dimensions of the sample chamber upon heating at the given nominal pressure. Considering these results, in the further analysis we assume quasi-isochoric conditions in the sample chamber upon temperature changes of $\Delta T = 80$ K. We also note that Chou *et al* [19] assumed perfect isochoric conditions in their high-pressure DAC experiments on H_2O within a 35 K range.

The Raman spectra were obtained at stabilized p–T conditions and used for the identification of different ice polymorphs, as well as for the study of pressure- and temperature-induced shifts of Raman frequencies (to be presented elsewhere). Figures 2 and 4 show representative Raman spectra and images of four phases of H_2O observed in this study, respectively.

3. Results

Figure 5 shows several p–T paths observed during the heating/cooling cycles. The occurrence of phase transitions and presence of thermal pressure are clearly manifested in the plot. At high pressure, water supercools deeply into the stability field of ice VII (cooling experiments w8 and w7) as well as into the field of ice VI (not shown). It is interesting to note that the p–T

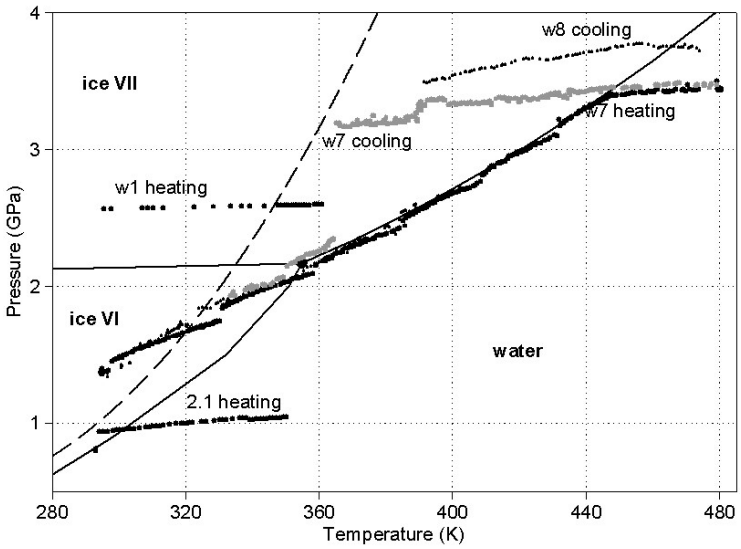

Figure 5. Examples of pressure–temperature paths during the heating/cooling cycles. The dashed line represents the melting curve of a new phase of ice reported by Chou *et al* [19]. The melting curve of ice VII is taken from Datchi *et al* [17].

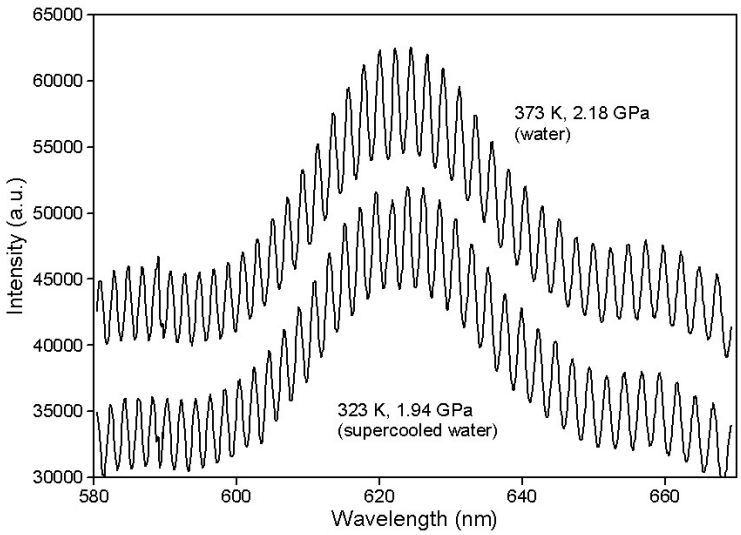

Figure 6. Interference fringes observed in the light transmitted through the layer of water confined between diamond anvils.

points of the precipitous drops of pressure (particularly for experiment w7 cooling) lie close to the melting curve of a new phase of ice (dashed curve in figure 5) reported by Chou *et al* [19]. The experimental runs which involved thermodynamic equilibrium between ice VII and water (experiment w7 heating) are in agreement with the melting curve of ice VII determined by Datchi *et al* [17].

We have analysed pressure changes which occurred upon temperature increase/decrease and compared them with the pressure changes calculated from the published EOSs for water

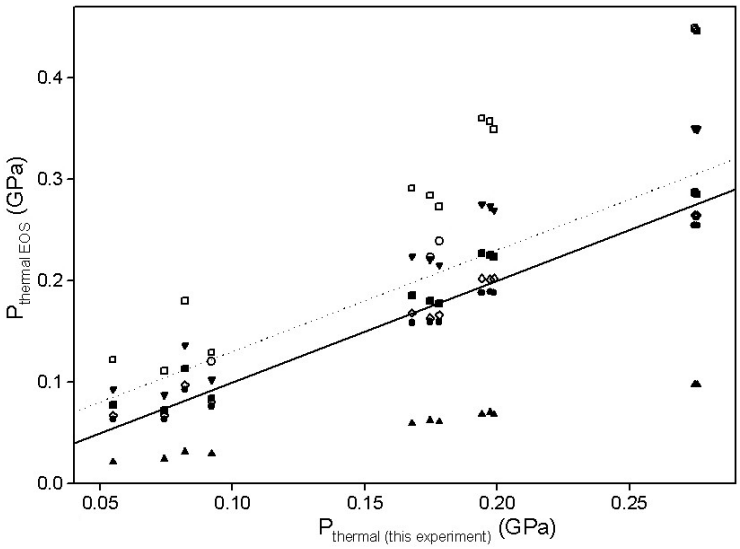

Figure 7. Comparison between thermal pressures determined in this study and those calculated from the published equations of state. Triangles up—[11], triangles down—[10], solid circles—[14], open circles—[8], solid squares—[9], open squares—[7], open diamonds–[12].

and ice VII under isochoric conditions. For water, the results are summarized in figure 7. The quality of the agreement between the experimental and the calculated points is given by their proximity to the diagonal solid line, which represents the maximum theoretical match. There is a good agreement with the EOSs given by Holland and Powell [9], Saxena and Fei [12, 13], and Halbach and Chatterjee [14], which also have the smallest standard deviations. We note, however, that the analysis of the interference fringes given above points to a minor thermal expansion of the sample volume, a deviation from the isochoric conditions corresponding to an approximate decrease of our experimental thermal pressure by about 0.03 GPa. To illustrate the consequences of this effect we shift the solid line of the best match in figure 7 by 0.03 GPa. The shifted line shows that the agreement with the published EOSs improves, except for the EOS given by Rimbach and Chatterjee [11]. However, the deviation from the EOS by Saul and Wagner [7] is still considerable for the upper range of the thermal pressure. The fundamental EOS of water by Saul and Wagner is described by 58 coefficients and is supposed to be accurate. This suggests that the deviation from the isochoric conditions in the sample chamber may be higher upon temperature scans exceeding a 50 K range.

The results of the thermal pressure analysis for ice VII are given in table 2. The experimentally determined thermal pressures are systematically lower by about 0.04 GPa as compared to those calculated from the EOS of ice VII by Fei *et al* [20]. This difference is explained by the quasi-isochoric experimental conditions and/or by the accuracy of the published EOS. For ice VII, the deviation from the isochoricity by 0.24% of volume corresponds to a pressure change of about 0.08 GPa in the 2–4 GPa range.

Following the sudden freezing of supercooled water, accompanied by the precipitous drop of pressure (e.g. cooling experiments w7 and w8), equilibrium of ice VII and water was observed in several experiments. By using EOSs of water and of ice VII we determined the percentage of water and ice VII in the sample chamber in eight experiments. We used the following equation:

$$V_{\mathrm{L}}(P_1, T) = xV_{\mathrm{L}}(P_2, T) + (1 - x)V_{\mathrm{VII}}(P_2, T),$$

Table 2. Experimental and calculated thermal pressures for ice VII. The calculated values are derived from the EOS [20].

Exp no.	T-range (K)	P_{init} (GPa)	ΔP_{exp} (GPa)	ΔP_{EOS} (GPa)
w9	302–346	2.74	0.055	0.100
w10	305–345	2.61	0.057	0.095
w11	321–360	3.16	0.068	0.114
w12	305–340	2.75	0.047	0.080
STD				0.041

Table 3. Calculated amount of ice VII coexisting with liquid water after the precipitous freezing of supercooled water in the stability field of ice VII (see, for example, cooling experiments w7 and w8 in figure 5). HC-EOS [14], SF-EOS [13], HP-EOS [9].

P (GPa)	T (K)	vol% of ice VII			ΔP_{exp} (GPa)
		HC	SF	HP	
3.49	390	31	22	35	0.94
4.14	439	28	23	32	0.77
3.84	423	25	20	29	0.72
3.35	373	20	18	22	0.58
3.31	378	19	15	22	0.57
3.39	375	24	14	28	0.72
3.98	434	22	18	25	0.61
4.30	451	23	16	27	0.61

where $V_L(P_1, T)$ is the volume of water just before the freezing and $V_L(P_2, T)$ and $V_{VII}(P_2, T)$ are the volumes of water and of ice VII, respectively, immediately after freezing (table 3). Our optical observations of the relative amounts of ice VII and water agree with the calculated results but a more quantitative analysis of the image was not possible due to the lack of information on the amounts of ice and H_2O in the axial direction due to visual limitations.

We observed interesting melting behaviour when slowly increasing temperature along the equilibrium line between ice VII and water (heating experiment w7 in figure 5), which is documented in figures 4(a)–(c). Just before their disappearance, the crystals of ice VII became very plastic and their shape changed to stripes and doughnuts, which rapidly moved and bent in a fashion resembling the movement of living bacteria. The plasticity of ice near melting originates from the progressive breaking of hydrogen bonds and the consequent weakening of bulk forces. At some point close to a transition, the surface (interfacial) energy becomes dominant and controls the shape of crystals. A similar phenomenon has been observed in the melting of NH_3 ice [21].

4. Conclusions

Our study on phase equilibria and EOSs of H_2O shows that the simultaneous use of two optical pressure sensors (Al_2O_3:Cr^{3+} and SrB_4O_7:Sm^{2+}) along with the thermocouple readings provides two independent means for accurate pressure and temperature determination. The conclusion about the reliability of the two methods is based on the p–T agreement between the observed phase transformations and the published phase diagram of H_2O, while the consistency of the two methods is proved by the close values of pressures and temperatures they provided.

The important conclusion of this study is that the various published p–V–T EOSs of H_2O ices and water (as well as of other fluids and soft solids) can be reliably checked for

mutual consistency, and even independently derived by the method of optical-pressure-sensor manometry in the DAC. This possibility originates from the isochoric-to-quasi-isochoric conditions in the sample chamber as well as from the fact that a small deviation from the isochoricity upon heating can be monitored by the method of interference fringes. In this respect it should noted that the accuracy of the analysis presented in this work can be significantly increased if one interference pattern is recorded for each fluorescence spectrum used for the pressure determination. This will provide the necessary information in order to compensate for the non-perfect isochoric conditions, assuming that a lateral dimension of the sample chamber remains unchanged, or is tracked by a high-resolution imaging. The limits of the ultimate resolution and applicability of this method to the determination of the EOS are most likely imposed by a reaction of the fluid under investigation with the metallic gasket, particularly at high temperatures. Here the choice of chemically resistant gasket material (e.g. Re, Re with Au insert) will play a critical role.

The cross-check between different EOSs can be accomplished by a method of systematic determination of thermal pressure as a function of pressure and temperature $P_{\mathrm{therm}}(p, T)$ as shown in this study. The complete determination of the EOS will require availability of reference volumes $V(p, T)$, such as those given by room-temperature p–V isotherms determined by x-ray diffraction, or reference volumes of well known invariant (triple) and univariant (phase lines) points on a phase diagram. This approach to the derivation of the p–V–T EOS is particularly valuable for fluids where the direct determination of density by x-ray diffraction from the radial distribution function still represents a novel technique requiring complex and difficult analysis [22]. Moreover, synchrotron radiation is needed for the low-Z materials like H_2O.

One potentially distinct advantage of the current approach is that the same technique can be used for the determination of EOSs of both fluid and liquid phases of the same sample in one experiment. This implies the same systematic errors (if present) in the EOSs of coexisting phases, i.e. internally self-consistent experimental data. Such datasets and EOSs are highly desirable for thermodynamic calculations, where the consistency results in a much higher precision of calculated phase boundaries due to the cancellations of systematic errors in the equation $G_{\mathrm{Phase1}}(p, T) = G_{\mathrm{Phase2}}(p, T)$, $G(p, T)$ being the Gibbs free energy at pressure p and temperature T [23].

The best agreement between our experimental data and the published EOSs is for the EOSs given by Holland and Powell [9], Saxena and Fei [12, 13], and Halbach and Chatterjee [14], while the EOS derived by Rimbach and Chatterjee [11] is not consistent with the results of this study. The agreement of data with the EOS of ice VII given by Fei *et al* [20] is good if the underestimation of the thermal pressure due to the quasi-isochoric conditions is taken into account.

Acknowledgments

We thank Dr Ch Chateau for providing the powder for the strontium borate sensor, and F Westman for help with the experimental set-up. We are also grateful to a careful anonymous reviewer whose comments and suggestions significantly contributed to the improvement of the original manuscript. The Swedish Research Council (Vetenskapsrådet) and Ångpanneföreningen's Foundation for Research and Development (Ångpanneföreningens Forskningsstiftelsen) are gratefully acknowledged for financial support (grants G-AA/GU 10592-307 and 02-142).

References

[1] Murakami M, Hirose K, Yurimoto H, Nakashima S and Takafuji N 2002 *Science* **295** 1885
[2] Bina C R and Navrotsky A 2000 *Nature* **408** 844
[3] Barr A C, Pappalardo R T and Stevenson D J 2001 *Lunar Planet. Sci.* **32**
[4] Consolmagno G J 1983 *J. Phys. Chem.* **87** 4204
[5] Spohn T and Schubert G 2003 *Icarus* **161** 456
[6] Kuskov O L, Kronrod V A and Saxena S K 2003 *Earth Planet. Sci. Lett.* submitted
[7] Saul A and Wagner W 1989 *J. Phys. Chem. Ref. Data* **18** 1537
[8] Wiryana S, Slutsky L J and Brown J M 1998 *Earth Planet. Sci. Lett.* **163** 123
[9] Holland T and Powell R 1991 *Contrib. Mineral. Petrol.* **109** 265
[10] Pitzer K S and Sterner S M 1994 *J. Chem. Phys.* **101** 3111
[11] Rimbach H and Chatterjee N D 1987 *Phys. Chem. Minerals* **14** 560
[12] Saxena S K and Fei Y 1987 *Geochim. Cosmochim. Acta* **51** 783
[13] Saxena S K and Fei Y 1987 *Contrib. Mineral. Petrol.* **95** 370
[14] Halbach H and Chatterjee N D 1982 *Contrib. Mineral. Petrol.* **79** 337
[15] Datchi F, LeToullec R and Loubeyre P 1997 *J. Appl. Phys.* **81** 3333
[16] Lacam A and Chateau C 1989 *J. Appl. Phys.* **66** 366
[17] Datchi F, Loubeyre P and LeToullec R 2000 *Phys. Rev.* B **61** 6535
[18] Dewaele A, Eggert J H, Loubeyre P and LeToullec R 2003 *Phys. Rev.* B **67** 094112
[19] Chou I M, Blank J G, Goncharov F, Mao H K and Hemley R J 1998 *Science* **281** 809
[20] Fei Y, Mao H K and Hemley R J 1993 *J. Chem. Phys.* **99** 5369
[21] Lazor P, Hemley R J and Mao H K 1996 *APS 1996 March Mtg (St Louis, MO, 1996)*; *Bull. Am. Phys. Soc.* **41** 564
[22] Eggert J H, Weck G, Loubeyre P and Mezouar M 2002 *Phys. Rev.* B **65** 174105
[23] Saxena S K, Chatterjee N, Fei Y and Shen G 1993 *Thermodynamic Data on Oxides and Silicates* (Berlin: Springer)